Deferoxamine as adjunct therapeutics for tuberculosis

Sandeep R. Kaushik,[1] Nidhi Yadav,[1] Sukanya Sahu,[1] Ashish Gupta,[1] Amit Kumar Mohapatra,[1] Adyasha Sarangi,[1] Swati Kumari,[2] Bichitra Biswal,[2] Ranjan Kumar Nanda[1,*]

[1]Translational Health Group, International Centre for Genetic Engineering and Biotechnology, New Delhi- 110067, India.

[2]Structural and Functional Biology Laboratory, National Institute of Immunology, New Delhi-110067, India.

Short title: Deferoxamine limits Mycobacterial growth

***Corresponding author**

Ranjan Kumar Nanda (PhD)

Translational Health Group, International Centre for Genetic Engineering and Technology, New Delhi-110067, India

Telephone: 91-11-26741358; E mail: ranjan@icgeb.res.in

Abstract: Iron is an essential element for the survival of both host and pathogens. Dysregulated iron metabolism is reported in tuberculosis patients, providing an opportunity for developing host-directed therapeutics. This study explored the antimycobacterial properties of an iron chelator, i.e. Deferoxamine (DFO), and its impact on limiting host iron on *Mycobacterium tuberculosis* (Mtb) and infected C57BL/6 mice. A group of mice received ferric carboxymaltose to create an iron overload condition and aerosol infected with H37Rv Mtb. A subgroup of Mtb-infected mice received isoniazid (INH) and rifampicin (RIF) with or without DFO for tissue CFU assay and liver metabolite analysis using mass spectrometry. DFO was shown to have comparative antimycobacterial properties like INH in *in-vitro* conditions. Iron-overloaded mice exhibited significantly higher tissue (lungs, liver, spleen) mycobacterial burden at two weeks post-infection, and the efficacy of INH and RIF were compromised. Iron chelation by DFO alone significantly reduced the tissue mycobacterial burden at four weeks post-treatment and, as an adjunct to INH and RIF, significantly lowered lung mycobacterial load within the first and second weeks of treatment compared to the group that received INH and RIF. The intracellular pro-inflammatory cytokine (IFN-γ, TNF-α and IL-17A) levels in the lung $CD4^+$ T-cells of INH and RIF-treated groups with or without DFO were found to be similar. DFO with RIF and INH treatment significantly altered liver arginine biosynthesis, which has a direct role in neutralizing ammonia and has an immune-supportive role. Currently, DFO is used for treating acute iron toxicity and thalassemic patients with iron overload and holds promise as an adjunct therapeutic candidate for tuberculosis.

Keywords: Tuberculosis, Iron overloading, Iron chelation, Deferoxamine, Host-directed therapeutics, Metabolomics.

Introduction: Tuberculosis (TB) is caused by *Mycobacterium tuberculosis* (Mtb) and affects multiple host tissues, including the lungs.[1] The duration of treatment modalities for TB patients infected with drug-sensitive Mtb strains is 6-9 months and may take up to 24 months or more if infected with drug-resistant strains.[2] Shortening the treatment duration in TB with additional host-directed therapeutics might increase adherence, reduce the relapse rate, and minimise drug resistance development, which may save millions of lost lives every year due to TB.[3]

Iron supplementation in TB patients is reported to worsen clinical outcomes and iron chelation in *in-vitro* and *in-vivo* settings significantly reduces Mtb load. [4,5,6,7,8,9] *Streptomyces pilosus* produces deferoxamine (DFO), which acts as a siderophore, has a strong affinity against iron (Fe^{3+}), and forms a stable feroxamine complex. DFO binds to non-transferrin-bound iron, which may limit the sequestering of free host iron required by Mtb for survival**.** In this study, we report that DFO has mycobactericidal properties and accelerates Mtb clearance in C57BL/6 mice in early time points in combination with the existing anti-TB drugs. DFO could be a promising adjunct therapeutic for TB and may help in reducing treatment duration for improved patient outcomes.

Methodology

Ethical statement: All the experiments adopted in this study were approved by the Institute Biosafety Committee and the Institute Animal Ethics Committee (ICGEB/IAEC/07032020/TH-11) of the International Center for Genetic Engineering and Biotechnology, New Delhi.

Mycobacterial H37Rv culture: *Mycobacterium tuberculosis* H37Rv strain (OD ≈ 0.02) were inoculated in 7H9 media (BD Difco Middlebrook) supplemented with glycerol (0.2%), tween 80 (0.05%) and OADC (Oleate, albumin dextrose and catalase, 10%) in the absence or presence of individual drugs or combination in the tuberculosis aerosol challenge facility (TACF, BSL-

III) at ICGEB New Delhi. Mtb were grown at 37°C in a shaker incubator set at 180 rpm. Individual drug solutions were prepared at their minimum inhibitory concentrations (MICs) for DFO (0.1 mg/ml) and isoniazid (INH, 0.1 µg/ml) using Milli-Q water. Mtb growth was monitored by measuring absorbance at 600 nm at an interval of 24 hours up to 5 days post-inoculation using a spectrophotometer to monitor the bactericidal activity of the drugs. The harvested control and drug-treated Mtb were inoculated on 7H11 plates for colony forming unit (CFU) assay on the fifth day. On the fifth day, a fraction of the Mtb culture (~0.8 OD, 133 M) were centrifuged at 3,500 g for 10 minutes at room temperature, and the pellet was harvested with the cultured media as a separate fraction for elemental analysis using inductively coupled plasma mass spectrometry (ICP-MS) analysis (Figure 1A).

Transmission electron microscopy of Mtb: Mtb cultures (OD ≈ 0.1) were inoculated with DFO, INH, and Gallium nitrate (GN, 4 µg/ml) at MIC and control, incubated at 180 rpm at 37°C. Mtb cultures were harvested five days post-treatment and centrifuged at 3,500 g for 5 minutes, followed by washing with phosphate buffer saline (PBS) by spinning at 3,500 g for 5 minutes. The pellet containing Mtb was fixed with 2% glutaraldehyde for an hour. The fixed bacterial pellet was washed twice with PBS and two washes with a 26 G needle five times to make a single-cell resuspended in 100 µl ddH_2O and passed through a 26 G needle for five times to make a single cell suspension. 10 µl suspension was loaded onto a carbon grid and stained with 5% uranyl acetate. After air drying the grid, it was loaded in the Transmission Electron Microscope (Tecnai G2 spirit, HT120kV), and micrographs were captured (Figure 1 E).

Kill kinetics of Mtb in the presence of DFO, GN, INH and their combination: Mtb H37Rv culture in their log phase (OD ≈ 0.2) was inoculated in 7H9 media (2 ml) supplemented with OADC (10 %), glycerol (0.2 %) and tween-80 (0.05 %) in presence of 10 × MIC of DFO (1 mg/ml), GN (40 µg/ml), INH (1 µg/ml) and their combination (DIG: DFO +INH + GN) and

were incubated at 37ºC at 180 rpm. Aliquots (100 µl) of each culture condition were harvested at days 0, 4 and 8 for CFU assay by plating diluted samples on 7H11 agar plates supplemented with OADC (10 %) and PANTA and incubated at 37ºC. Mycobacterial colonies were enumerated after three weeks post-plating.

J774A.1 infection with H37Rv and DFO treatment: The J774A.1 cells were seeded on sterile round cover glass in a six-well plate. The cells were pretreated with different DFO concentrations (0, 0.25, 2.5 and 25 mM) for 24 hours before introducing Mtb H37Rv at multiple of infection (MOI) of 1:10. After washing, the cells were stained with DAPI (1 µg/ml, Invitrogen #D1306), MitoTracker™ Red CMXRos (200 nM, Invitrogen #M7512) and fixed at different time points and finally slides were prepared for confocal microscopy by using the prolong gold antifade mountant (Invitrogen, Cat# P36934). These fixed cells were used for fluorescence microscopy using a Laser scanning confocal microscope (Nikon A1R, USA), and images were analyzed using NIS-Element software.

Atomic structure analysis of the iron storage proteins in *Mycobacterium tuberculosis*: The atomic coordinates of the 3D structures of known iron storage proteins in Mtb, i.e., both BfrA (Rv1876) and BfrB (Rv3841) were obtained from the Protein Data Bank (www.rcsb.org).[10,11,12] The 3D structures of BfrA and BfrB were analyzed, and figures were made using Pymol molecular visualization software.[13]

Iron supplementation in C57BL/6 mice and Mtb aerosol infection: C57BL/6 mice (8-10 weeks old, male) from the host (ICGEB) animal house were transferred to the tuberculosis aerosol challenge BSL-III facility (TACF) for adaptation for at least one week before the infection experiment. The animals were kept in a specific pathogen-free environment, 12-hour daylight conditions, and food and water were provided ad libitum. A set of the study mice received ferric-carboxymaltose (Ferinject, LUPIN ltd, India, 0.5 mg iron/mice in 100 µl saline)

through intravenous injection, while the control mice received saline (100 µl). These iron-supplemented mice received four doses of ferric-carboxymaltose injections every fourth day. After a week of rest, the iron-supplemented and control mice were aerosol infected with a low dose (110-120 CFU) of Mtb H37Rv strain using Madison chamber present in TACF and sacrificed at 15-, 45- and 90-days post-infection (dpi) to monitor for tissue bacterial load. A subgroup of Mtb infected C57BL/6 mice received either INH-RIF (InIR, 0.1 g/l each, changed alternate day) in drinking water ad-libitum or DFO (InD, 150 mg/Kg body weight of mice, intraperitoneal injection) or both (InIRD) starting 15 dpi for 75 days (i.e., 90 dpi). DFO dose was introduced intraperitoneally every third day till treatment completion. At the end of the study, mice were anaesthetized using 5% Isoflurane, and organs were harvested from the humanely euthanized mice. Harvested tissues (lungs, spleen, and liver) were processed using a homogenizer in sterile PBS (1 ml). An aliquot (100 µl) of it was inoculated on 7H11 agar plates at appropriate dilution in sterile PBS, and the colonies were counted after three weeks of incubation at 37°C in the incubator. To a part of liver tissue, harvested on 45 dpi, chilled methanol was added and stored at -80°C for elemental analysis using ICP-MS.

Sex as a biological variable: Since females are more prone to disturbed iron metabolism and anemia due to physiological loss of blood, so male mice were used in this study.

Tissue histology analysis: A part of the harvested tissues was stored in 10% formaldehyde for histology analysis. Briefly, processed tissues were paraffin-embedded, and 5 µm thickness sections were used for slide preparation at an accredited pathology lab. Prussian blue staining was used to monitor tissue iron distribution.

Elemental analysis using ICP-MS: To the harvested Mtb pellet (OD ≈ 0.8, ~133 million), HNO_3 (70%, 150 µl) was added and transferred to sample vials (MG5, Anton Paar, USA) and H_2O_2 (30%, 50 µl) was added. Similarly, to the culture filtrates (~1 ml), HNO_3 (70%, 500 µl) and H_2O_2 (30%, 150 µl) were added. The sealed sample vials were subjected to microwave

(Anton Paar, USA) digestion using a ramp of 250W for 15 min with a hold time of 5 min at 250W. Similarly, liver (~50 mg) tissues were taken in a digestion vial (64MG5 vials) and, after adding HNO_3 (400 µl) and H_2O_2 (100 µl), were incubated for 20 min at room temperature. Then, the vials were sealed and subjected to microwave digestion. The initial power was set at a ramp of 10 min and 150W with a max temperature of 140ºC, followed by a 15 min hold. Then, a second ramp of 15 min from 150-250W was used, and a final hold was to bring the temperature to 55ºC at the highest fan speed. After diluting the samples with trace metal-free water, iron (57Fe) levels were monitored in the digested samples using ICP-MS (iCAPTM TQ ICP-MS, Thermo Scientific, USA). Thermo Scientific Qtegra Intelligent Scientific Data Solution (ISDS) software operated and controlled the instrument. Briefly, the torch was warmed up for 30 min in single-quad Kinetic energy discrimination (SQ-KED) mode with helium to remove the polyatomic nuclei interference and then autotuned in normal mode followed by advanced KED mode. Then, the multi-element standard (#92091, Sigma Aldrich, USA) of different concentrations was run at the same settings to prepare the standard plot. A sample blank was run, followed by each sample, and a quality control (QC) of known concentrations of standards was run after every 15-20 samples to monitor and maintain uniform signal intensity throughout the complete run. Data analysis was done using Qtegra software (Thermo Scientific, USA).

Liver metabolite profiling using GC-TOF: Liver tissues (~100 mg) were finely chopped and transferred to bead-beating tubes (2 ml) with zirconium beads (2 mm, ~250 mg). Chilled methanol (80%, 1 ml) was added to the tubes and ribitol (5 µl, 2 mg/ml) as a spike in standard. The tissues were subjected to bead beating using Biospec Mini-Beadbeater-16 at 3650 oscillations/minute, 30 seconds on/off cycles for six times with incubation on ice during the off cycle. After bead beating, the samples were incubated on ice for 30 minutes and then centrifuged at 10,000 g for 10 minutes at 4 °C to collect the supernatant (~800 µl). The

extracted metabolites were filtered (0.2 µm, nylon membrane filter #726-2520) and stored at -20 °C until further processing. An equal volume (~120 µl) of extracted metabolites from all samples from a particular time point were pooled to prepare a QC.

For derivatization, samples were dried at 40 °C using a vacuum concentrator (Labconco Centrivap, USA) and incubated with Methoxamine hydrochloride (MeOX-HCl, 2%, 40 µl) at 60 °C for 2 hours at 900 rpm in a thermomixer (Eppendorf, USA). After adding N-methyl-N-(trimethylsilyl), trifluoroacetamide (MSTFA, 60 µl) was incubated at 60 °C for 30 minutes at 900 rpm in a thermomixer. After incubation, the samples were centrifuged at 10,000 g for 10 minutes at 25 °C, the supernatant was transferred to GC vial inserts for GC-MS analysis using a 7890 Gas Chromatography (Agilent Technologies, Santa Clara, CA) coupled to a Pegasus 4D GC × GC time-of-flight mass spectrometer (LECO Corporation). All samples were randomized using a Research Randomizer (www.randomizer.org) and processed in a batch of 20 samples per day with one QC sample each at the beginning, middle and end of the sequence. The derivatized samples (1 µL) were injected into an HP-5ms GC column (30 meters length, 250 µm internal diameter**)** in splitless mode using Helium as a carrier gas at a constant flow rate (1 ml/min), and the secondary column was Rxi-17 of 1.5 m length and 250µm diameter. Electron ionization (EI) mode was fixed at −70 eV to scan ions of 33 to 600 m/z range at an acquisition rate of 20 spectra/second. The ion source temperature was set at 220 °C. GC method parameters used for acquisition were: 50 °C for 1 minute, ramp of 8.5 °C/min to 200 °C, ramp of 6 °C/ min to 280 °C, hold for 5 minutes. The secondary oven temperature offset was set at 5 °C relative to the GC oven temperature. Similarly, the modulator temperature offset was set at 15 °C close to the secondary oven temperature. The transfer line temperature was set at 225 °C. A solvent delay of 600 seconds was used, and all data acquisition was completed within 24 hours of derivatization. A commercial standard mix of organic acids and amino acids was derivatized and run using the same GC-MS method to confirm the identity of the important

metabolic features. All GC-MS raw data files of the study groups were aligned using the "Statistical Compare" feature of ChromaTOF (4.50.8.0, Leco, CA, USA). Peaks with a width of 1.3 seconds and a signal-to-noise ratio (S/N) threshold of 50 were selected. The putative identity of the peaks was assigned using a NIST (National Institute of Standards and Technology, USA) library (version 11.0; 243,893 spectra) search, qualifying a similarity match of >600 at a mass threshold of 100. The .csv file, generated from the above analysis, was manually curated to check the peak identity. Analytes present at least in 50% of the samples of a study group were selected for statistical analysis. The Ribitol peak area from the sample was used for normalizing the liver metabolite data, fold change analysis and p-value were calculated using Metaboanalyst software version 6.0. Metabolic features that showed $\log_2$ Fold change $\geq \pm 1.0$ with p-value < 0.05 between the study groups were selected as deregulated important molecules. Pathway enrichment analysis for deregulated molecules was performed using the Pathway analysis plugin in the Metaboanalyst software.

Intracellular cytokine staining and flow cytometry analysis: The right lobes of the lungs were harvested and incubated with collagenase (1 mg/ml) and DNase (1 mg/ml) in RPMI-1640 (2 ml) at 37 °C for 30 min. The enzymatically treated tissues were passed through a strainer (70 µm) before centrifuging at 400 g for 10 min to collect the pellet. Ammonium chloride potassium (ACK) lysis buffer was added to the pellet, incubated for 2 min at room temperature (RT) and quenched by adding RPMI-1640. After pelleting, these cells were resuspended in RPMI-1640 after counting, were seeded in a 12-well plate and incubated overnight with phorbol 12-myristate 13-acetate (5 ng, PMA) and ionomycin (0.75 µg). After washing, these cells were incubated with brefeldin (5 µg) and monensin (1.3 µg) for 3 hrs. The cells were washed with FACS buffer (1% FBS in PBS) and incubated with an antibody cocktail of LIVE/DEAD, CD3 and CD4 surface markers (Live dead fixable stain #L34975, CD3-FITC #11-0032-82 and CD4-Bv780 #100552 from Invitrogen, USA) for 40 mins on ice. After

staining, these cells were fixed using paraformaldehyde (4%) and permeabilized using Permeabilization buffer (#00-8333-56, Invitrogen, USA). These cells were incubated with an antibody cocktail of intracellular cytokines like TNF-α, IL-17A and IFN-γ (TNF-α APC #17-7321-82, IL-17A efluor450 #48-7177-82, IFN-γ PerCP Cy5.5 #45-7311-82 from Invitrogen, USA). Flow cytometry data were acquired using BD LSR Fortessa X-20 (Supplementary Figure S8A) and analyzed using FCSExpress (DeNovo software, Version 6.0, India).

Statistical analysis: All data were presented as mean ± Standard error of the mean (SEM) values. Statistical analyses were performed using Origin 2020 and Microsoft Excel using an unpaired two-tailed t-test to identify group-specific variations. Statistical differences were considered significant with $p<0.05$ at 95% confidence.

Results

Deferoxamine affects mycobacterial growth in vitro*:* Iron chelation in Mtb H37Rv by DFO leads to compromised growth in a time-dependent manner (Figure 1B). The growth kinetics of Mtb in the presence of DFO in 7H9 media were comparable to INH-treated groups (Figure 1B). Furthermore, the combined treatment of DFO and INH also compromised Mtb growth kinetics. At day five post-inoculation, a significant reduction in the Mtb survival was observed in the presence of either DFO or INH or their combination (Figure 1C). However, as expected, DFO alone or combined with INH significantly reduced intracellular Iron levels in Mtb (Figure 1D). The substantial reduction in intracellular Iron, zinc and copper levels (data not shown for copper and zinc) might contribute to the bactericidal effect. For its survival and growth, Mtb relies on these divalent ions for various processes like two-metal ion catalysis essential for its survival and growth.

Electron micrographs of Mtb treated with DFO and INH-RIF, harvested on day five post-treatment, showed changes in cell wall compared to the control and Gallium nitrate (GN) treated Mtb (Figure 1F). The kill kinetics of DFO were comparable to INH (Figure 1G). The

CFU count on day 4 with DFO treatment was significantly higher than INH, indicating the lower initial bactericidal activity for DFO. But this became comparable by day eight post-inoculation (Figure 1H and 1I). Gallium nitrate (GN) exhibited a less pronounced bactericidal effect than DFO and INH, so we excluded it from further experiments. These results revealed the notable impact of DFO on limiting Mtb growth, and its effect was enhanced in the presence of existing anti-TB drugs like INH. The primary factor contributing to the bactericidal activity of DFO is its substantial influence on restricting the availability of iron for the mycobacteria.

DFO shows anti-mycobacterial activity in Mtb-infected J774A.1 cell culture: The fluorescence images of the Mtb-infected J774A.1 cells that received DFO treatment or control were analyzed using NIS-Element software. The DFO pretreated J774A.1 cells showed decreased intracellular mycobacterial burden in a dose-dependent manner (Supplementary figure S1A). Interestingly, we also observed hypertrophy in DFO-treated cells. We analyzed the 3D structure of iron storage proteins of Mtb, i.e., BfrA: Rv 1876 and BfrB: Rv3841 and observed that the biological units of both BfrA and B contain 24 submits arranged in a 432 molecular symmetry. Further, BfrA harbors 48 iron atoms and 12 heme moieties, whereas no iron atom has been incorporated into the 3D structure of BfrB. However, likely, BfrB would also contain 48 iron molecules in locations similar to those in BfrA (Supplementary Figure S1C, D, E and F).

Iron supplementation leads to liver iron loading, higher tissue mycobacterial load and compromised efficacy of INH and RIF: The methods adopted for iron supplementation/overloading are presented in Supplementary Figure S2A. Iron supplementation/overloading had a negligible effect on the mice's body weight during and after the course (Supplementary Figure S2C). However, the iron-overloaded mice group showed significantly higher liver iron levels than the control group (Supplementary Figure S2D). Prussian blue staining of the liver samples of iron-overloaded groups also showed higher

iron accumulation and distribution (Supplementary Figure S2B). Thigh muscle iron levels of iron-overloaded mice didn't show significant variations (Data not shown). The tissue (lungs, spleen, and liver) mycobacterial burden was significantly higher in the iron-overloaded mice group at 15 days post-infection compared to the controls (Supplementary Figure S3E, F and G). The liver iron levels of iron-overloaded groups were significantly higher than control groups, and INH-RIF treatment had a marginal effect on it (Supplementary Figure S3A, S3B). Prussian blue staining and ICP-MS of liver samples obtained from iron-overloaded mice groups showed higher iron accumulation till 75 days post-treatment (Supplementary Figure S3C, D). As expected, the INH-RIF treatment cleared the tissue mycobacterial burden in control groups; however, the mycobacterial clearance in the lungs and spleen of iron-overloaded mice groups was delayed and took longer time (>30 days of treatment) to bring it to lower than the limit of detection (Supplementary Figure S3E, F, G). Interestingly, the liver mycobacterial burden of the iron-overloaded group was similar to the control groups at 45 and 90 days post-infection. This demonstrates that higher host iron levels compromise the anti-mycobacterial efficacy of commonly used anti-TB drugs like INH and RIF.

Iron chelation by DFO significantly reduced the tissue mycobacterial burden in C57BL/6 mice: Mtb infected C57BL/6 mice treated with DFO alone showed significant reduction in the liver iron levels in both iron-supplemented as well non-supplemented conditions and also reflected in Prussian blue staining (Figure 2B, 2C). The decrease in iron levels followed by a significant reduction in lung Mtb load within 30 days post-treatment was observed and continued up to 75 days post-treatment (90 dpi) compared to the infected control in non-supplemented groups (Figure 2D). Similar observations were found in the livers of DFO-treated mice, but the spleen CFU remained similar (Figure 2E, 2F). Interestingly, DFO treatment in the Mtb-infected iron-overloaded mice group was ineffective in reducing tissue

mycobacterial burden at an early point (30 days post-treatment). In contrast, a decreasing trend was observed in the lung and liver tissues by 75 days post-treatment (Figure 2F, 2D).

DFO adjunct to anti-tuberculosis drugs aids in early lung mycobacteria clearance and alters liver metabolome: Significantly lower liver iron levels were observed in the DFO-treated mice with or without RIF-INH treatment (InIR, Figure 3B, C). DFO adjunct to ani-tuberculosis drugs (INH and RIF; InIRD) showed no difference in lung bacterial burden at 30 days post-treatment (Figure 3D). Interestingly, Mtb infected C57BL/6 mice treated with DFO adjunct to INH-RIF (InIRD) showed a significant reduction in lung mycobacterial burden even at early time points, i.e., one- and two-weeks post-treatment compared to the INH-RIF (InIR) treated group (Figure 3F, I). Liver metabolome analysis using GC-MS showed 20 deregulated ($\log_2$ Fold change $>\pm 1.0$; p-value< 0.05) metabolic features between the InIRD vs InIR group at the first week of treatment completion. DFO treatment altered the liver's Alanine, Glutamic acid, Lactic acid and malonic acid levels (Figure 3G). Pathway enrichment analysis showed an overrepresentation of Alanine, Aspartate and Glutamate metabolism, pyruvate metabolism and Arginine biosynthesis (Figure 3J). Organic acids like pantenoic acid, lactic acid and alloxanoic acid were deregulated in the liver of drug-treated mice (both InIR and InIRD) as compared to the infected control (In) at the first week of treatment (Supplementary Figure S4A and B). Similarly, seven deregulated metabolic features were identified in the liver of the DFO-treated group completing two weeks of treatment (Figure 3J). The InIRD group had significantly higher levels of proteogenic amino acids (Valine and Isoleucine) and non-proteinogenic amino acids (Ornithine and Aminoadipic acid) compared to the InIR group (Figure 3J). Arginine biosynthesis was overrepresented in the livers of mice receiving DFO adjunct to RIF- and INH (Figure 3H, K). Long-chain fatty acids like oleic acid, arachidonic acid and octadecanoic acid were deregulated in the liver of the drug-treated mice (InIR, InIRD) as compared to the infected control (In) in the second week of treatment (Supplementary Figure

S4C, D). The arachidonic acid pathway was overrepresented in the treatment groups in the first week. In contrast, biosynthesis of unsaturated fatty acids (linoleic and alpha-linoleic acid) was increased in treated groups compared to the infected controls. The drug metabolism pathway for INH metabolism was enriched in the treated groups (Supplementary Figure S5).

IFN-γ, TNF-α and IL-17 production in lung $CD4^+$ T-cells of INH and RIF with and without DFO-treated C57BL/6 mice were similar: Frequency of lung $CD3^+CD4^+$ cells were similar in Mtb infected C57BL/6 mice receiving INH-RIF with or without DFO at two weeks post-treatment. (Supplementary Figure S6B). The intracellular pro-inflammatory cytokine (IFN-γ, TNF-α and IL-17A) levels in the lung $CD4^+$ T-cells of INH and RIF-treated groups with or without DFO were found to be similar (Supplementary Figure S6C).

Discussion: Numerous biological processes, including cell wall synthesis, ATP synthesis, DNA coiling, transcription, and translation in Mtb, have been instrumental in developing anti-TB drugs.[14] However, limited studies have attempted to understand how iron overloading conditions in hosts affect Mtb growth and influence the effectiveness of anti-TB agents. Additionally, the effect of iron limitation on the survival ability of Mtb has received less attention.[15,16] In this study, we attempted to generate evidence of the pivotal role played by host iron in Mtb survival and how manipulating iron availability through chemical agents, such as iron chelators, may impact Mtb clearance in both in-vitro and in vivo settings.

Mtb cultured in 7H9 media supplemented with DFO exhibited notable bactericidal activity akin to the effectiveness of INH. The observation of our *in-vitro* study aligns with previous reports and corroborates the anti-mycobacterial role of DFO.[7] Iron deprivation targets mycobacterial membrane integrity by enhancing membrane permeability and disrupting membrane homeostasis reported in *M. smegmatis*.[9] Electron micrograph images of H37Rv Mtb treated with DFO and INH showed cell wall damage and a decreased envelope thickness compared to the controls (Figure 1F). DFO restricts intracellular iron levels but also impacts Copper and

Zinc levels. Furthermore, DFO influences the expression of iron storage proteins, such as BrfA/B and oxidative stress genes. DFO has been reported to increase glycolytic metabolism in Mtb-infected human monocyte-derived macrophages (hMDMs) while concurrently enhancing the early innate immune response by increasing the expression of IL-1β and TNF-α both at transcript and protein levels.[17] Importantly, DFO was observed to reversibly inhibit DNA synthesis in human B and T lymphocytes with limited impact on RNA and protein synthesis. In the presence of equimolar $FeCl_3$, the effects of DFO in these cells were also reversed.[18]

Iron supplementation in C57BL/6 mice had no discernible effect on weight gain, corroborating earlier reports in Sprague Dawley rat pups.[19] The liver plays a pivotal role in maintaining iron homeostasis by detecting even minor fluctuations in the systemic iron requirements and accumulating excess iron.[20] Various regulatory mechanisms within the liver govern the expression of the iron regulatory genes, storage capacity, and iron mobilization. Dysregulation of these functions can lead to iron imbalance, a primary contributor to iron-related disorders.

Several reports have shown that iron supplementation in mice, whether administered orally or parenterally, supports the growth of non-tuberculous mycobacteria (NTM). However, the studies on Mtb are limited and need additional investigation.[21] A preliminary study by Kochan *et al.* demonstrated that iron supplementation in mice significantly increased the Mtb burden in spleen and lung tissues.[22] Our study delved into the impact of host iron status on Mtb survival and growth *in-vivo*, revealing that intravenous administration of ferric carboxymaltose, a form of iron supplementation, promoted mycobacterial growth in lung, liver, and spleen several weeks post supplementation. However, this effect waned within a few months after discontinuing the supplementation.

Limiting iron through DFO administration to Mtb-infected mice significantly reduced liver iron levels and tissue mycobacterial burden compared to the infected control group.

Furthermore, liver iron levels in iron-overloaded C57BL/6 mice significantly declined upon DFO treatment. We also assessed the effect of DFO when used in conjunction with anti-TB drugs like INH and RIF. Significantly lower lung bacterial burden was observed between animals treated with INH and RIF with and without DFO. This suggests that DFO, as an adjunct to existing TB drugs, holds promise for potentially shortening the duration of anti-TB treatment. However, appropriate clinical studies are necessary for further validation. It is worth exploring whether DFO, as an adjunct, could also reduce the dosage of existing TB drugs, which presents an exciting avenue for future research.

Our findings underscore the role of DFO as an adjunct therapeutic agent for TB treatment, offering new insights into manipulating host iron metabolism to shorten the treatment duration. Host-directed therapies involving iron chelation merit further validation to determine their impact on limiting drug resistance development, if any. Particular attention should be given to the potential toxicity of DFO treatment, bearing in mind that it showed that introducing an equivalent amount of $FeCl_3$ in cellular systems negates its function.[19] Additionally, DFO is an FDA-approved drug with pro-inflammatory properties and is utilized in humans for conditions like hemochromatosis.[23] Here, we have demonstrated the role of DFO as an adjunct therapeutic in reducing the Mtb burden by limiting iron availability in the C57BL/6 mice. Although, male mice were used in this study, iron chelation in both sexes will limit Mtb growth.

Anti-tuberculosis drug treatment leads to drug-induced liver injury (DILI). Our results showed that the arginine biosynthesis pathway was enriched in the DFO-treated group, which could contribute to liver detoxification.[24] Arginine is an essential anti-oxidant for the liver and is reported to neutralize ammonia, leading to liver detoxification. Its supplementation is reported to help in liver regeneration.[25] Arginine, Alanine and Valine were upregulated in the liver of DFO-treated mice with potential immune-supportive functions. Alanine is converted to pyruvate by the alanine aminotransferase (ALT) enzyme in the liver, which contributes to

glucose production by gluconeogenesis and enhances immune cell function against pathogens (Figure 4H).[26] Our results show it enriched linoleic acid and alpha-linoleic acid metabolism along with arachidonic acid metabolism in the treated groups compared to infected controls at the first and second week of treatment- Linoleic acid is also a precursor for arachidonic acid, which gives rise to an essential class of inflammatory mediators called eicosanoids to elicit an immune response against pathogens.

The combined effects of DFO with first-line anti-TB drugs could yield enhanced bactericidal effects and potentially lead to a reduction in the duration of TB treatment. Recently, a study by Cahill *et al.* demonstrated that DFO treatment in BCG-infected primary hMDMs resulted in increased bactericidal activity of bedaquiline, indicating the potential of DFO to have additive effects with the second-line anti-TB drugs.[7] Further research is required to assess the efficacy of DFO in combination with these drugs against drug-resistant Mtb isolates. The pro-inflammatory role of DFO includes enhancing transcript and protein levels of IFN-γ, IL-1β and TNF-α in Mtb-infected hMDMs.[7] But, interestingly, we did not observe any significant changes in the intracellular cytokine levels (IFN-γ, IL-17A and TNF-α) in $CD4^+$ T-cells harvested from the lungs of Mtb-infected C57BL/6 mice when treated with DFO in combination with first-line anti-TB drugs (Supplementary figure S8). DFO is reported to restore glycolytic capacity in the Mtb-infected hMDMs by increasing HIF-1α expression and inhibiting IDO1 expression, which might not have a direct effect on the pro-inflammatory pathways, including Th1 and Th17 as per our flow cytometry results from in-vivo experiments.

The mechanism involved in the mycobactericidal activity of DFO is mediated by different pathways in *in-vivo* conditions. The reported increased pro-inflammatory cytokine production *in vitro,* which needs additional investigation.

Targeting other critical trace elements like copper, zinc and Mmgnesium, essential for Mtb survival and growth, could also be a promising avenue for TB treatment.[27,28,29] Additionally,

exploring the role of gene polymorphisms in NRAMP1, HFE (associated with hemochromatosis), HP and β2 macroglobulin genes, which contribute to TB susceptibility, may facilitate the identification of the populations that could benefit the most from iron chelation therapy. [4,30]

Currently, there is no effective TB vaccine available for adults, and drug-resistant TB cases have been on the rise. Incorporating therapeutic agents that enhance the efficacy of existing chemotherapeutics can significantly reduce morbidity and mortality associated with TB. Several FDA-approved drugs have emerged as potential host-directed therapeutic candidates for combination therapy with the existing TB drugs. Our findings, along with those of others, suggest that DFO administration bolsters host immunity, leading to improved Mtb control and, therefore, has the potential to serve as an agent for host-directed adjunct therapy. These new therapeutic interventions targeting host or pathogen iron metabolism, such as iron chelation, are poised to contribute to the fight against TB.

Online supplemental material: Five supplementary figures are available in the Supplemental file.

Acknowledgements: We acknowledge the Department of Biotechnology (DBT), Government of India, for supporting activities through research grants and supporting the Tuberculosis Aerosol Challenge Facility at ICGEB and the ICGEB New Delhi for providing access to the ICP-MS facility and core support to RKN. Sandeep R. Kaushik received a Senior Research Fellowship from the DBT, and Sukanya Sahu received a Senior Research Fellowship from the Council of Scientific and Industrial Research (CSIR) New Delhi. Nidhi Yadav and Ashish Gupta received a Junior Research Fellowship from the DBT. We thank Ms Mothe Sravya for helping prepare the manuscript.

Authorship Contributions: SRK and RKN conceptualized and designed experiments; SRK, SS, AKM, NY and AG performed the animal experiments; SRK, SS, AKM, NY, AG, and AS carried out in-vitro and the laboratory profiling experiments; SRK, NY analyzed data and prepared figures. SK and BB took care of the Mtb protein structure study; RKN generated funds for this work; SRK and RKN wrote the first draft of the manuscript and revised it, incorporating the comments of all co-authors.

Disclosure of Conflicts of Interest: All authors declare no conflict of interest.

References

1. https://www.cdc.gov/tb/topic/basics/default.htm (accessed on 31/05/2023)

2. Revised National Tuberculosis Control Programme (RNTCP) https://tbcindia.gov.in/WriteReadData/NSP Draft 20.02.2017 1.pdf (accessed on 31/05/2023)

3. Hawn TR, Matheson AI, Maley SN, Vandal O. Host-directed therapeutics for tuberculosis: can we harness the host? Microbiol Mol Biol Rev. 2013 Dec;77(4):608-27.

4. Boelaert JR, Vandecasteele SJ, Appelberg R, Gordeuk VR. The effect of the host's iron status on tuberculosis. J Infect Dis. 2007 Jun 15;195(12):1745-53.

5. Phelan JJ, Basdeo SA, Tazoll SC, McGivern S, Saborido JR, Keane J. Modulating iron for metabolic support of TB Host Defense. Front Immunol. 2018 Oct 15;9:2296.

6. Lounis N, Maslo C, Boelaert JR, Bonnafous P, Trnffot-Pernot C, Baohong J, Grosset J. Impact of iron loading and iron chelation on murine tuberculosis. Clinical Microbiology and Infection. 199; 5 (11):687-692.

7. Cahill C, O'Connell F, Gogan KM, Cox DJ, Basdeo SA, O'Sullivan J, Gordon SV, Keane J, Phelan JJ. The iron chelator desferrioxamine increases the efficacy of bedaquiline in primary human macrophages infected with BCG. Int J Mol Sci. 2021 Mar 13;22(6):2938.

8. Schaible UE, Collins HL, Priem F, Kaufmann SH. Correction of the iron overload defect in beta-2-microglobulin knockout mice by lactoferrin abolishes their increased susceptibility to tuberculosis. J Exp Med. 2002 Dec 2;196(11):1507-13.

9. Pal R, Hameed S, Fatima Z. Iron deprivation affects drug susceptibilities of Mycobacteria targeting membrane integrity. J Pathog. 2015;2015:938523.

10. McMath LM, Contreras H, Owens CP, Goulding CW. The structural characterization of bacterioferritin, BfrA, from Mycobacterium tuberculosis. J. Porphyrins Phthalocyanines 2013; 17, 229–239.

11. Khare G, Gupta V, Nangpal P, Gupta RK, Sauter NK, Tyagi AK. Ferritin structure from Mycobacterium tuberculosis: comparative study with homologues identifies extended C-terminus involved in ferroxidase activity. PLoS One. 2011 Apr 8;6(4):e18570.

12. wwPDB consortium. Protein Data Bank: the single global archive for 3D macromolecular structure data. Nucleic Acids Res. 2019 Jan 8;47(D1):D520-D528.

13. DeLano W L. The PyMOL molecular graphics system. http://www.pymol. org (2002).

14. Horsburgh CR, Barry E, Lange C. Treatment of Tuberculosis. N Engl J Med 2015; 373:2149-2160

15. Theriault ME, Pisu D, Wilburn KM, Lê-Bury G, MacNamara CW, Michael Petrassi H, Love M, Rock JM, VanderVen BC, Russell DG. Iron limitation in M. tuberculosis has broad impact on central carbon metabolism. Commun Biol. 2022 Jul 9;5(1):685.

16. Rodriguez GM. Control of iron metabolism in Mycobacterium tuberculosis. Trends Microbiol. 2006 Jul;14(7):320-7.

17. Phelan JJ, McQuaid K, Kenny C, Gogan KM, Cox DJ, Basdeo SA, O'Leary S, Tazoll SC, Ó Maoldomhnaigh C, O'Sullivan MP, O'Neill LA, O'Sullivan MJ, Keane J. Desferrioxamine supports metabolic function in primary human macrophages infected with Mycobacterium tuberculosis. Front Immunol. 2020 May 13;11:836.

18. Lederman HM, Cohen A, Lee JW, Freedman MH, Gelfand EW. Deferoxamine: a reversible S-phase inhibitor of human lymphocyte proliferation. Blood. 1984 Sep;64(3):748-53.

19. McMillen S, Lönnerdal B. Postnatal iron supplementation with ferrous sulfate vs. ferrous is-glycinate chelate: Effects on iron metabolism, growth, and central nervous system development in sprague dawley rat pups. Nutrients. 2021 Apr 22;13(5):1406.

20. Anderson ER, Shah YM. Iron homeostasis in the liver. Compr Physiol. 2013 Jan;3(1):315-30.

21. Agoro R, Mura C. Iron supplementation therapy, a friend and foe of Mycobacterial infections? Pharmaceuticals (Basel). 2019 May 17;12(2):75.

22. Kochan I. The role of iron in bacterial infections, with special consideration of host-tubercle bacillus interaction. Curr Top Microbiol Immunol. 1973;60:1-30.

23. Parker JB, Griffin MF, Downer MA, Akras D, Berry CE, Cotterell AC, Gurtner GC, Longaker MT, Wan DC. Chelating the valley of death: Deferoxamine's path from bench to wound clinic. Front Med (Lausanne). 2023 Feb 15;10:1015711.

24. Jeong I, Park JS, Cho YJ, Yoon HI, Song J, Lee CT, Lee JH. Drug-induced hepatotoxicity of anti-tuberculosis drugs and their serum levels. Journal of Korean medical science. 2015 Feb 1;30(2):167-72.

25. Lee DY, Kim EH. Therapeutic effects of amino acids in liver diseases: current studies and future perspectives. Journal of Cancer Prevention. 2019 Jun;24(2):72.

26. Qian K, Zhong S, Xie K, Yu D, Yang R, Gong DW. Hepatic ALT isoenzymes are elevated in gluconeogenic conditions including diabetes and suppressed by insulin at the protein level. Diabetes/metabolism research and reviews. 2015 Sep;31(6):562-71.

27. Mehdiratta K, Singh S, Sharma S, Bhosale RS, Choudhury R, Masal DP, Manocha A, Dhamale BD, Khan N, Asokachandran V, Sharma P, Ikeh M, Brown AC, Parish T, Ojha AK, Michael JS, Faruq M, Medigeshi GR, Mohanty D, Reddy DS, Natarajan VT, Kamat SS,

Gokhale RS. Kupyaphores are zinc homeostatic metallophores required for colonization of Mycobacterium tuberculosis. Proc Natl Acad Sci U S A. 2022 Feb 22;119(8):e2110293119.

28. Piddington DL, Kashkouli A, Buchmeier NA. Growth of Mycobacterium tuberculosis in a defined medium is very restricted by acid pH and Mg(2+) levels. Infect Immun. 2000 Aug;68(8):4518-22.

29. Dow A, Sule P, O'Donnell TJ, Burger A, Mattila JT, Antonio B, Vergara K, Marcantonio E, Adams LG, James N, Williams PG, Cirillo JD, Prisic S. Zinc limitation triggers anticipatory adaptations in Mycobacterium tuberculosis. PLoS Pathog. 2021 May 14;17(5):e1009570.

30. Li X, Yang Y, Zhou F, Zhang Y, Lu H, Jin Q, Gao L. SLC11A1 (NRAMP1) polymorphisms and tuberculosis susceptibility: updated systematic review and meta-analysis. PLoS One. 2011 Jan 25;6(1):e15831.

Figure Legends

Figure 1: Deferoxamine (DFO) chelates iron and shows mycobactericidal effect in the in-vitro culture. **A.** Schematic presentation of the method used for in-vitro Mtb culture with DFO and isoniazid (INH) for growth kinetics, ICP-MS. **B.** Growth kinetics of *Mycobacterium tuberculosis* H37Rv strain in the absence and presence of different drugs (DFO, INH, DFO+INH) and in control. **C.** Survived Mycobacteria cultures on day 5 post-drug-treated conditions and control as observed in colony forming unit **(**CFU) assay, showing the significant bactericidal effect of the drugs alone or in combination. **D.** Intracellular elemental levels in drug-treated and controlled Mycobacterial culture at 5th-day post-treatment quantified using ICP-MS. **E.** Schematic presentation of the methodology used for TEM sample preparation. **F.** Transmission electron micrographs of untreated, DFO treated, INH, Gallium nitrate (GN) treated Mtb, respectively harvested at 5th day post drug treatment. **G.** Kill curve of Mtb with DFO, GN, INH and combination (DFO + GN + INH), at 10× MIC of each drug **H.** CFU plot for day 4 post-inoculation**.** CFU plot for day 8 post-inoculation ns: not significant; *: $p<0.05$; **: $p<0.01$; ***: $p<0.001$; ****: $p<0.005$ at 95% confidence interval

Figure 2: DFO aids in Mycobacterial clearance in C57BL/6 mice A. Schematic presentation of the method used to infect C57BL/6 mice with *Mycobacterium tuberculosis* H37Rv strain and treated using DFO. **B.** Liver iron levels were estimated using ICP-MS in the infected control compared with Mtb-infected mice receiving DFO treatment. **C.** Prussian Blue stained liver histology for DFO-treated non-supplemented mice. Mycobacterial load in lungs **(D)**, spleen **(E)** and liver **(F)** of control and DFO treated *Mycobacterium tuberculosis* H37Rv infected C57BL/6 mice. n = 5/group/time points; i.p.: intra-peritoneal injection; dpi: days post infection; wpi: weeks post-infection, CFU: colony forming units; *: $p<0.05$; **: $p<0.01$; ***: $p<0.00$; p-values at 95% confidence interval.

Figure 3: DFO helps in the early clearance of Mtb in adjunct to anti-tuberculosis drugs (INH and RIF) and leads to alterations in the host liver metabolome. **A.** Schematic presentation of the method used for Mycobacterial infection and treatment using INH and RIF with or without DFO. **B.** Prussian blue staining of the liver tissue of IRD-treated mice (InIRD) showing decreased iron accumulation as compared to infected IR-treated mice **C** Liver iron levels, estimated using ICP-MS, in the infected controls and infected mice receiving INH and RIF with DFO. **D.** Lung mycobacterial load of the *Mycobacteria tuberculosis* H37Rv infected C57BL/6 mice receiving INH and RIF with or without DFO. **E.** Schematic presentation of the method used for Mycobacterial infection, treatment using INH and RIF with or without DFO and monitoring host tissues at early time points **F.** Lung mycobacterial load one wpt. **G.** Liver metabolome of Mycobacterial infected mice treated with anti-tuberculosis drugs with DFO vs without DFO at the first week of treatment. **H.** Scatter dot plot showing pathway enrichment analysis of deregulated metabolic features from **G** plot. **I.** Lung mycobacterial load two wpt. **J.** Liver metabolome of Mycobacterial infected mice treated with anti-tuberculosis drugs with DFO vs without DFO at the second week of treatment. **K.** Scatter dot plot showing pathway enrichment analysis of deregulated metabolic features from **J** plot. n = 5/group/time points; i.p.: intra-peritoneal injection; dpi: days post-infection; wpi: weeks post-infection, wpt: weeks post-treatment, CFU: colony forming units; *: $p<0.05$, ns: not significant; up: upregulated, down: downregulated, p-values at 95% confidence interval.

Figure 4: Effect of iron overload vs iron chelation on in-vitro Mtb culture, Mtb infected cell culture and different tissues of Mtb infected mice.

Figure 1

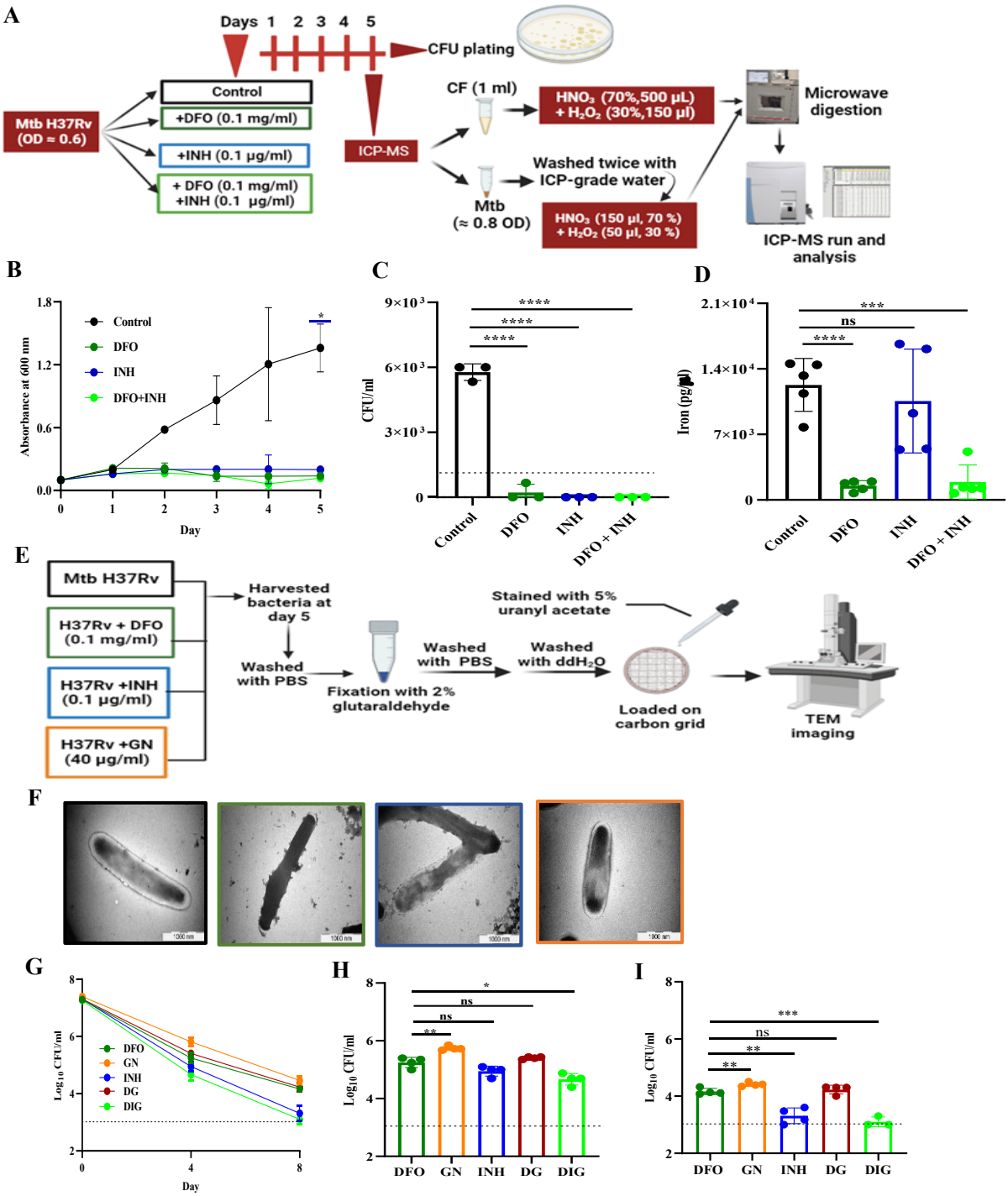
A
Days 1 2 3 4 5
CFU plating
Mtb H37Rv (OD ≈ 0.6)
Control
+DFO (0.1 mg/ml)
+INH (0.1 µg/ml)
+ DFO (0.1 mg/ml) +INH (0.1 µg/ml)
ICP-MS
CF (1 ml)
HNO₃ (70%,500 µL) + H₂O₂ (30%,150 µl)
Microwave digestion
Washed twice with ICP-grade water
Mtb (≈ 0.8 OD)
HNO₃ (150 µl, 70 %) + H₂O₂ (50 µl, 30 %)
ICP-MS run and analysis
B
Absorbance at 600 nm
Control
DFO
INH
DFO+INH
Day
C
CFU/ml
Control
DFO
INH
DFO + INH
D
Iron (pg/µl)
Control
DFO
INH
DFO + INH
E
Mtb H37Rv
H37Rv + DFO (0.1 mg/ml)
H37Rv +INH (0.1 µg/ml)
H37Rv +GN (40 µg/ml)
Harvested bacteria at day 5
Washed with PBS
Fixation with 2% glutaraldehyde
Washed with PBS
Washed with ddH₂O
Stained with 5% uranyl acetate
Loaded on carbon grid
TEM imaging
F
G
Log₁₀ CFU/ml
DFO
GN
INH
DG
DIG
Day
H
Log₁₀ CFU/ml
DFO
GN
INH
DG
DIG
I
Log₁₀ CFU/ml
DFO
GN
INH
DG
DIG

Figure 2

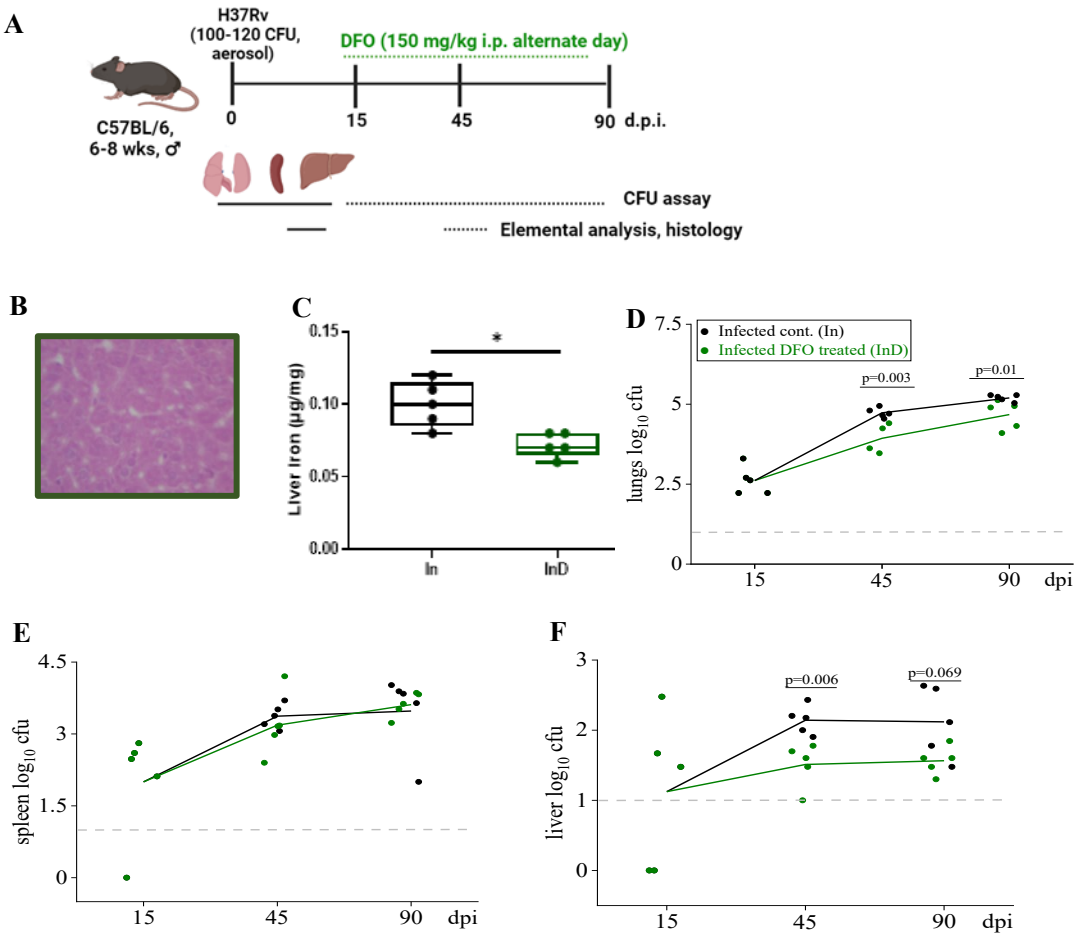
A
H37Rv
(100-120 CFU,
aerosol)
DFO (150 mg/kg i.p. alternate day)
C57BL/6,
6-8 wks, ♂
0
15
45
90 d.p.i.
CFU assay
Elemental analysis, histology
B
C
Liver Iron (µg/mg)
0.15
0.10
0.05
0.00
*
In
InD
D
Infected cont. (In)
Infected DFO treated (InD)
lungs log10 cfu
7.5
5
2.5
0
p=0.003
p=0.01
15
45
90
dpi
E
spleen log10 cfu
4.5
3
1.5
0
15
45
90
dpi
F
liver log10 cfu
3
2
1
0
p=0.006
p=0.069
15
45
90
dpi

Figure 3

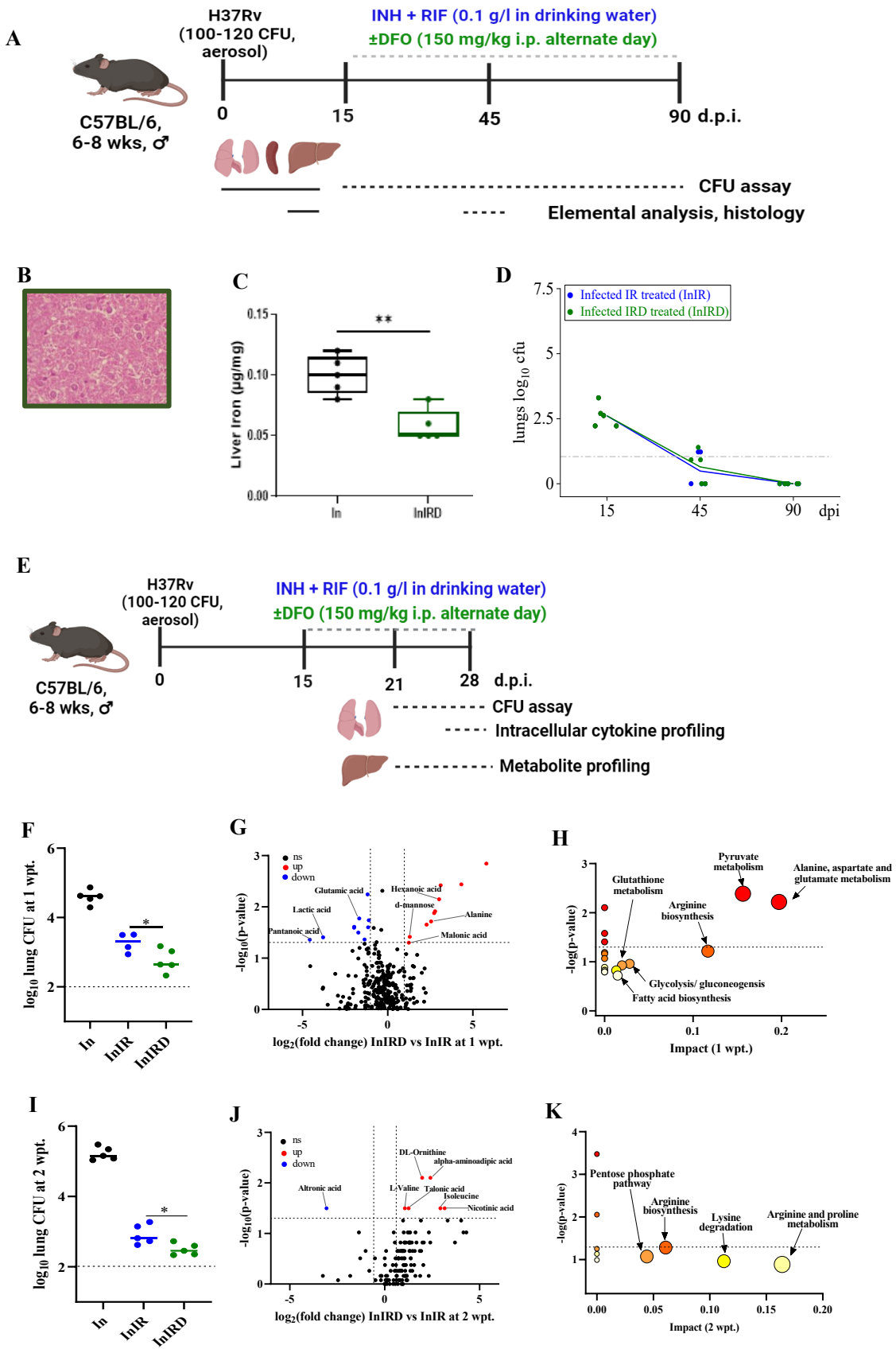
A
H37Rv
(100-120 CFU,
aerosol)
INH + RIF (0.1 g/l in drinking water)
±DFO (150 mg/kg i.p. alternate day)
C57BL/6,
6-8 wks, ♂
0
15
45
90 d.p.i.
CFU assay
Elemental analysis, histology
B
C
Liver Iron (µg/mg)
In
InIRD
D
Infected IR treated (InIR)
Infected IRD treated (InIRD)
lungs log10 cfu
dpi
E
H37Rv
(100-120 CFU,
aerosol)
INH + RIF (0.1 g/l in drinking water)
±DFO (150 mg/kg i.p. alternate day)
C57BL/6,
6-8 wks, ♂
0
15
21
28 d.p.i.
CFU assay
Intracellular cytokine profiling
Metabolite profiling
F
log10 lung CFU at 1 wpt.
In
InIR
InIRD
G
ns
up
down
Glutamic acid
Hexanoic acid
Lactic acid
d-mannose
Alanine
Pantanoic acid
Malonic acid
-log10(p-value)
log2(fold change) InIRD vs InIR at 1 wpt.
H
Pyruvate metabolism
Alanine, aspartate and glutamate metabolism
Glutathione metabolism
Arginine biosynthesis
Glycolysis/ gluconeogensis
Fatty acid biosynthesis
-log(p-value)
Impact (1 wpt.)
I
log10 lung CFU at 2 wpt.
In
InIR
InIRD
J
ns
up
down
DL-Ornithine
alpha-aminoadipic acid
Altronic acid
L-Valine
Talonic acid
Isoleucine
Nicotinic acid
-log10(p-value)
log2(fold change) InIRD vs InIR at 2 wpt.
K
Pentose phosphate pathway
Arginine biosynthesis
Lysine degradation
Arginine and proline metabolism
-log(p-value)
Impact (2 wpt.)

Figure 4

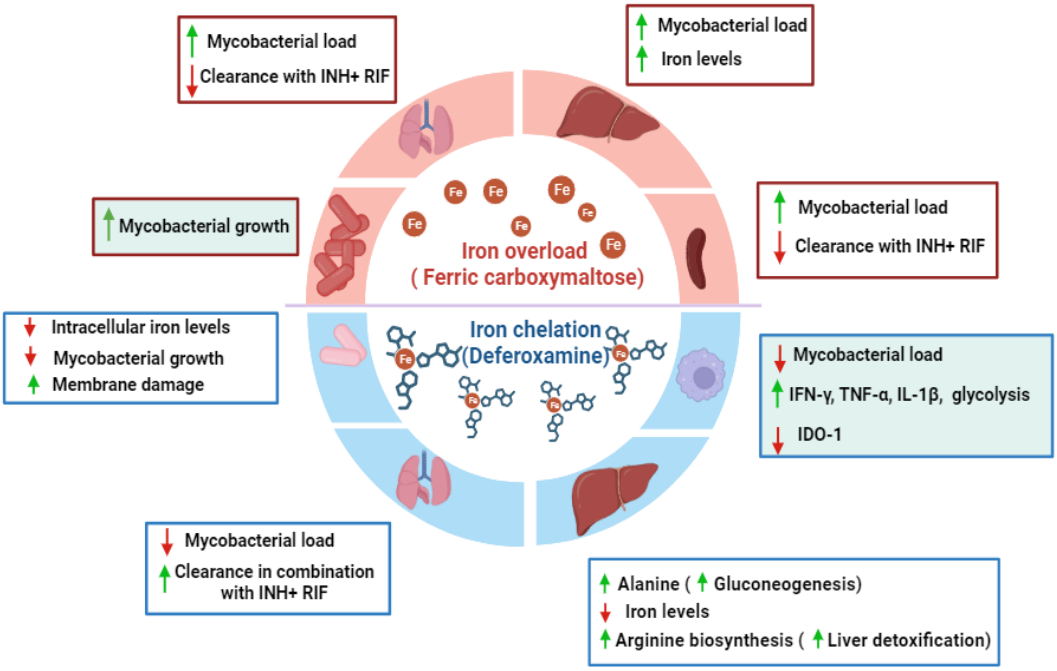
Mycobacterial load
Clearance with INH+ RIF
Mycobacterial load
Iron levels
Mycobacterial growth
Mycobacterial load
Clearance with INH+ RIF
Iron overload
(Ferric carboxymaltose)
Intracellular iron levels
Mycobacterial growth
Membrane damage
Iron chelation
(Deferoxamine)
Mycobacterial load
IFN-γ, TNF-α, IL-1β, glycolysis
IDO-1
Mycobacterial load
Clearance in combination with INH+ RIF
Alanine (Gluconeogenesis)
Iron levels
Arginine biosynthesis (Liver detoxification)